JVS

Effects of aluminum on the reduction of neural stem cells, proliferating cells, and differentiating neuroblasts in the dentate gyrus of D-galactose-treated mice via increasing oxidative stress

Sung Min Nam[1,2], Jong Whi Kim[1,2], Dae Young Yoo[1,2], Woosuk Kim[1,2], Hyo Young Jung[1,2], Jung Hoon Choi[3], In Koo Hwang[1,2,4], Je Kyung Seong[1,2,4], Yeo Sung Yoon[1,2,4,*]

[1]Department of Anatomy and Cell Biology, [2]BK21 PLUS Program for Creative Veterinary Science Research, Research Institute for Veterinary Science, and
[4]Korea Mouse Phenotyping Center, College of Veterinary Medicine, Seoul National University, Seoul 08826, Korea
[3]Department of Anatomy, College of Veterinary Medicine, Kangwon National University, Chuncheon 24341, Korea

Aluminum (Al) accumulation increases with aging, and long-term exposure to Al is regarded as a risk factor for Alzheimer's disease. In this study, we investigated the effects of Al and/or D-galactose on neural stem cells, proliferating cells, differentiating neuroblasts, and mature neurons in the hippocampal dentate gyrus. $AlCl_3$ (40 mg/kg/day) was intraperitoneally administered to C57BL/6J mice for 4 weeks. In addition, vehicle (physiological saline) or D-galactose (100 mg/kg) was subcutaneously injected to these mice immediately after $AlCl_3$ treatment. Neural stem cells, proliferating cells, differentiating neuroblasts, and mature neurons were detected using the relevant marker for each cell type, including nestin, Ki67, doublecortin, and NeuN, respectively, via immunohistochemistry. Subchronic (4 weeks) exposure to Al in mice reduced neural stem cells, proliferating cells, and differentiating neuroblasts without causing any changes to mature neurons. This Al-induced reduction effect was exacerbated in D-galactose-treated mice compared to vehicle-treated adult mice. Moreover, exposure to Al enhanced lipid peroxidation in the hippocampus and expression of antioxidants such as Cu, Zn- and Mn-superoxide dismutase in D-galactose-treated mice. These results suggest that Al accelerates the reduction of neural stem cells, proliferating cells, and differentiating neuroblasts in D-galactose-treated mice via oxidative stress, without inducing loss in mature neurons.

Keywords: D-galactose, adult neurogenesis, aluminum, hippocampus, oxidative stress

Introduction

Animal studies of neurodegeneration are gaining attention with regard to chronic aluminum (Al) consumption because of its relationship with Alzheimer's disease (AD) [13,33]. Aluminum comprises 8% of the Earth's crust, and its wide utilization in daily life elevates its bioavailability [14,20]. Natural Al is found in water in low amounts, but acid rain has been causing an elevation of Al concentration in water [17]. Weathering of Al-containing crustal material and human activities such as mining and cultivation also contribute to the increased levels of Al in the environment [7,9]. Additionally, the chance of Al exposure has increased in response to the wide usage of Al in items such as cooking utensils, cosmetics, drinking containers, food additives, and pharmaceutical products. Al can be consumed by various routes, such as inhalation, ingestion, and dermal absorption, but its entry into the body is low for its excretion through urination [29]. Non-excreted Al is distributed throughout the body, ending up in bone, liver, kidney, brain, and the hematopoietic system. Al toxicity is not obvious at low doses, but quickly develops after accumulation. Al accumulated in the organs causes osteomalacia, anemia, hepatorenal destruction, and encephalopathy [1,20,29,31]. Furthermore, the concentration of Al in tissue increases with aging [31]. Aluminum is a trivalent metal like Fe and binds with transferrin in the blood, which is one of its main mechanisms of toxicity. Al can replace Fe, and this free form of Fe can then cause oxidative stress [4,40].

Among oxidative stressors, superoxide radicals are the most abundant and are capable of initiating biological membrane destruction by activating lipid peroxidation [25,35]. 4-Hydroxynonenal (4-HNE) is the end product of lipid peroxidation in the cell membrane, and its accumulation elicits impaired cellular function and subsequent cell death [21]. Superoxide dismutases (SODs) remove superoxide radicals and mainly exist in cells as cytosolic (Cu, Zn-SOD, SOD1), mitochondrial (Mn-SOD, SOD2), and extracellular (EC-SOD, SOD3) forms [5,38].

Oxidative stress is one mechanism of aging related phenotype [32]. An aging-like phenotype is induced by treatment of D-galactose (D-gal) for 6−10 weeks [6,18,22,26]. Additional long-term treatment with Al in this model enhances the amyloidogenic pathway [18]. The hippocampus and connected areas are vulnerable to AD-like pathology and are also associated with memory impairment [3,19] because adult neurogenesis in the dentate gyrus of the hippocampus is important for memory processes [23]. In the Al-treated rat brain, cognitive deterioration has been shown to be associated with hippocampal lesions, similar to lesion patterns found in the brains of AD patients [37]. Contrary to the non-transgenic AD model established via combined long-term treatment of Al and D-gal, there have been few studies of the effects of subchronic (4 weeks) Al exposure on hippocampal neurogenesis in D-gal-treated mice. Moreover, most studies of the effects of Al and D-gal have been conducted in Kunming mice, an outbred mouse strain in China. To understand the combined effects of Al and D-gal, we investigated the change in the process of neurogenesis from neural stem cells through their proliferation and differentiation to neurons in the hippocampal dentate gyrus. To determine whether any differences existed, we immunostained for the following marker proteins: nestin (a marker for neural stem cells), Ki67 (a marker for proliferating cells), doublecortin (DCX, a marker for differentiating neuroblasts), and NeuN (a marker for mature neurons). We also investigated the state of the lipid peroxidation and antioxidant enzymes in the hippocampus.

Materials and Methods

Experimental animals

We choose C57BL6J mice because they are the most widely used inbred strain and background strain for transgenic mice. Five-week-old male C57BL/6J mice were purchased from Japan SLC, Inc. (Shizuoka, Japan). Animals were housed under conventional conditions with adequate temperature ($23^{o}C$) and humidity (60%) on a 12-hour light-dark cycle. Free access to food and water were provided. The procedures for handling and caring of animals were conducted in accordance with the Guide for the Care and Use of Laboratory Animals issued by the Institute of Laboratory Animal Resources, USA, 1996, and the experimental protocol was approved by the Institutional Animal Care and Use Committee (IACUC) of Seoul National University (approval No. SNU-121119-3). All experiments were carried out in a manner that minimized the number of animals used and their suffering.

Drug treatment

Following a 1-week acclimation to laboratory conditions, the animals were divided into four groups ($n = 8$ in each group): vehicle-treated (vehicle), Al-treated (Al), D-gal-treated (D-gal), and Al-D-gal-treated (Al-D-gal). Animals were fed a commercially available chow diet for 4 weeks. In all groups, vehicle (deionized water, pH 6.7) or aluminum chloride ($AlCl_3$) was intraperitoneally administered to 6-week-old mice (40 mg/kg/day) once a day for 4 weeks. In addition, vehicle (physiological saline) or D-gal (100 mg/kg, Sigma, USA) was subcutaneously injected into these mice immediately after intraperitoneal treatment. This schedule was adopted because the Al-induced reduction of cell proliferation and neuroblast formation was detected at 4 weeks after the start of Al treatment in a previous study [28]. In addition, absorptive water soluble Al compound, $AlCl_3$, was used in the present study, and water pH was adjusted to achieve maximal solubility of Al [12,28,30]. The dose of D-gal and/or Al used in this study was determined in previous studies [6,26,28].

Body weight (BW), food intake and blood glucose levels

Body weight was measured every week on Monday morning and at the end of the experiment. Food intake was measured and corrected for spillage by weighing the jars containing food every week between 9:00 AM and 10:00 AM. Data are expressed as calories (cal)/day・BW (g). To measure blood glucose levels, blood was sampled 1 day before sacrifice (9:00 AM) by 'tail nick' and analyzed using a portable glucose monitor (ACCU-CHEK GO; Roche, Germany).

Tissue processing

At the end of the experiment, 10 week-old mice ($n = 8$ in each group) were anesthetized with 30 mg/kg Zoletil 50 (Virbac, France) and perfused transcardially with 0.1 M phosphate-buffered saline (PBS; pH 7.4) followed by 4% paraformaldehyde in 0.1 M phosphate-buffer (PB; pH 7.4). Brains were removed and postfixed in 4% paraformaldehyde in PB for 6 hours. For immunohistochemical staining, brain tissue was cryoprotected by infiltration with 30% sucrose in PBS overnight, embedded in OCT compound (Sakura Finetechnical, Japan) and stored at $-70^{o}C$. Next, 30 μm thick brain sections were serially cut in the coronal plane using a cryostat (Leica, Germany). Brain sections were selected between 1.46 mm and 2.46 mm posterior to the bregma for each animal with reference to a mouse atlas [10]. Above area is corresponding to the dorsal hippocampus, and we used only dorsal hippocampus for the different role of the newly

generated cells in dorsal and ventral hippocampus [8]. Sections 180 μm apart from each other were collected in six-well plates containing PBS and stored in storage solution until further processing.

Immunohistochemistry

Free-floating sections were carefully processed under the same conditions to obtain accurate data for immunohistochemistry. From each well, selected sections (every sixth section, 5 sections per mouse) 180 μm apart from each other were sequentially treated with 0.3% hydrogen peroxide (H_2O_2) in 0.1 M PBS and 10% normal goat or horse serum in 0.1 M PBS. The sections were then incubated with diluted chicken anti-nestin antibody (1 : 250; Novus, USA), rabbit anti-Ki67 antibody (1 : 1,000; Abcam, UK), goat anti-DCX antibody (1 : 50; Santa Cruz Biotechnology, USA), mouse anti-NeuN (1 : 1,000; Millipore, USA), mouse anti-4-HNE antibody (1 : 500; Alpha Diagnostic, USA), rabbit anti-SOD1 (1 : 100; StressMarq Biosciences, Canada) or rabbit anti-SOD2 (1 : 100; Millipore) overnight, and subsequently exposed to biotinylated goat anti-chicken IgG, goat anti-rabbit, rabbit anti-goat, or horse anti-mouse IgG (diluted 1 : 200; Vector Labs, USA) and streptavidin peroxidase complex (diluted 1 : 200, Vector Labs). Next, the sections were visualized by reaction with 3,3'-diaminobenzidine tetrahydrochloride (Sigma).

To quantitatively analyze the number of Ki67-, DCX-, and NeuN-positive cells in all groups, the corresponding areas were counted using an image analysis system equipped with a computer-based CCD camera (Optimas 6.5 software; CyberMetrics, USA). The cell counts from all sections were averaged.

The region of interest for nestin, DCX, 4-HNE, SOD1, and SOD2 immunoreactivity in the dentate gyrus was analyzed using an image analysis system. Images were calibrated into an array of 512×512 pixels corresponding to a total dentate gyrus (100× primary magnification). Pixel resolution was 256 gray levels. The intensity of nestin, DCX, 4-HNE, SOD1, and SOD2 immunoreactivity was evaluated by means the relative optical density (ROD), which was obtained after transforming the mean gray level using the formula: ROD = log (256/mean gray level). The ROD of the background was determined in unlabeled portions using the NIH Image 1.59 software and the value was subtracted for correction, yielding high ROD values in the presence of preserved structures and low values after structural loss. The ROD ratio was calibrated as a percentage.

Statistical analysis

Data represent the mean number of experiments performed for each experimental area. Differences among means were statistically analyzed using two-way analysis of variance followed by Bonferroni post-tests to elucidate differences among groups using the GraphPad Prism 5.0 software (GraphPad Software, USA). A $p < 0.05$ was considered significant.

Results

Effects of Al and/or D-gal on body weight, food intake, and blood glucose levels

Body weight and food intake tended to be higher in the non-Al-treated groups than the Al-treated groups during experiments. Body weight and food intake in the Al and Al-D-gal groups were lower than those in the vehicle and D-gal groups, respectively, and these differences were maintained
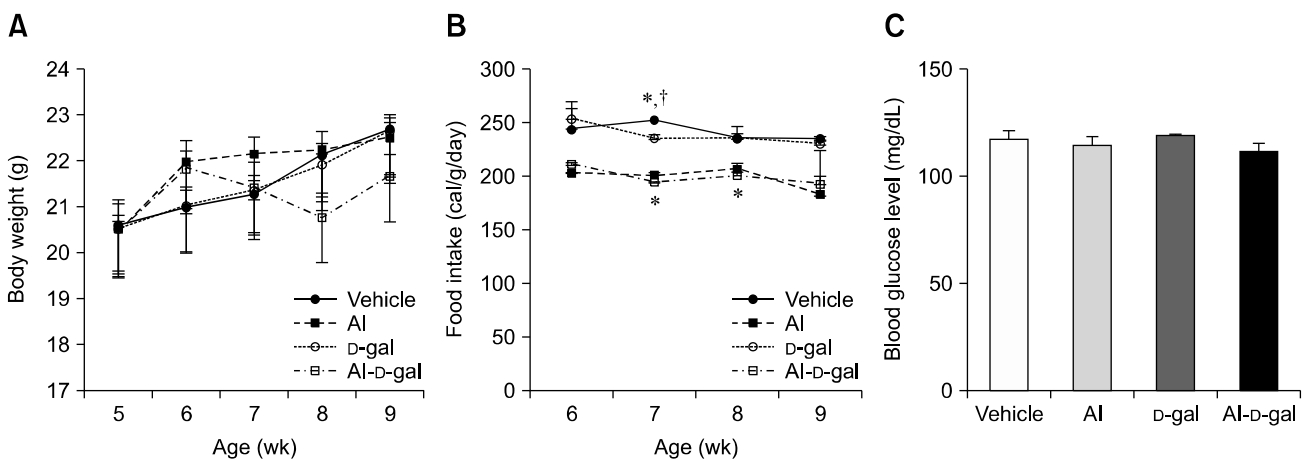

Fig. 1. Changes in body weight (A), food intake (B), and blood glucose levels (C) in the vehicle, aluminum (Al), D-galactose (D-gal), and aluminum-D-galactose (Al-D-gal) groups (n = 8 per group; *p < 0.05 indicates a significant difference between vehicle/vehicle-D-gal and Al/Al-D-gal, †p < 0.05 indicates a significant difference between vehicle/vehicle-Al and D-gal/Al-D-gal). Data are presented as the mean ± standard error of the mean (SEM).

throughout the experiment (panels A and B in Fig. 1). However, significant differences were found only in food intake at 7 and 8 weeks of age. The Al group ($p < 0.01$) and the D-gal group ($p < 0.05$) showed a prominent reduction in food intake compared to the Veh group at 7 weeks of age. In the Al-D-gal group, food intake was significantly decreased at 7 and 8 weeks of age ($p < 0.01$) (panels A and B in Fig. 1). Blood glucose levels did not differ significantly among groups (panel C in Fig. 1).

Effects of Al and/or D-gal on neural stem cells

In all groups, nestin-immunoreactive cells and fibers were detected in the subgranular zone and the granule cell layer of the dentate gyrus (panel A in Fig. 2). Nestin-immunoreactive cells

and fibers were decreased in the Al and D-gal groups compared to the vehicle group (panels B and C in Fig. 2). Nestin immunoreactivity decreased in the Al and D-gal groups to 83.68% ($p > 0.05$) and 84.04% ($p > 0.05$) of the vehicle group, respectively (panel E in Fig. 2). In the Al-D-gal group, nestin immunoreactivity decreased further, to 73.80% of the vehicle group; however, its level did not differ from those of the Al and D-gal groups ($p > 0.05$) (panels D and E in Fig. 2).

Effects of Al and/or D-gal on cell proliferation

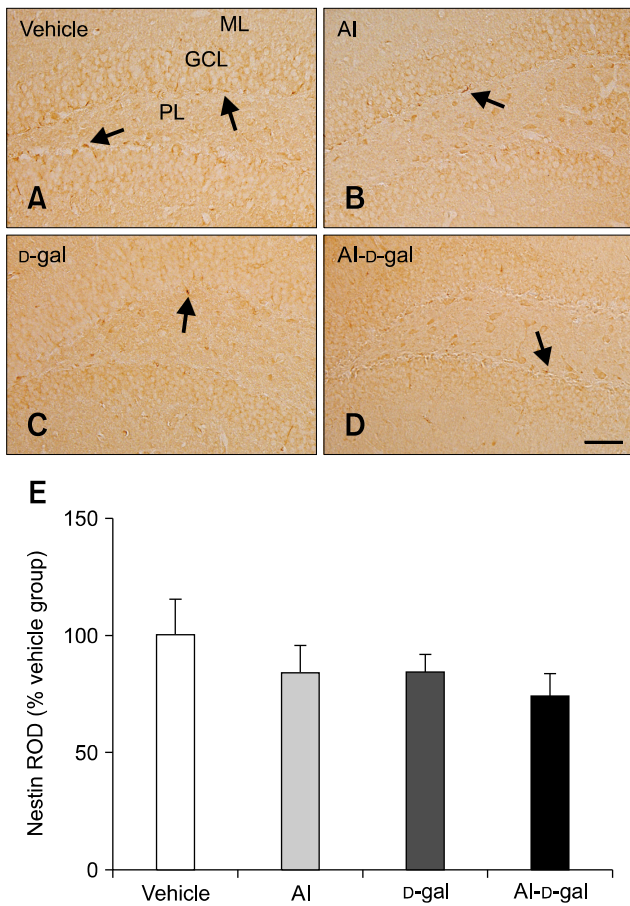In all groups, Ki67-immunoreactive nuclei were clustered

Fig. 2. Immunohistochemistry of nestin in the dentate gyrus of the vehicle (A), Al (B), D-gal (C), and Al-D-gal (D) groups. Nestin-immunoreactive cells and fibers decreased in the Al-D-gal and D-gal groups compared to the vehicle group. Nestin-immunoreactive cells and fibers decreased significantly in the Al-D-gal group compared to the vehicle group. (E) Relative optical density (ROD) demonstrated as percentages of vehicle group in nestin immunoreactivity per section in all groups ($n = 8$ per group). Data are presented as the mean ± SEM. GCL, granule cell layer; PL, polymorphic layer; ML, molecular layer. Scale bar = 50 µm.
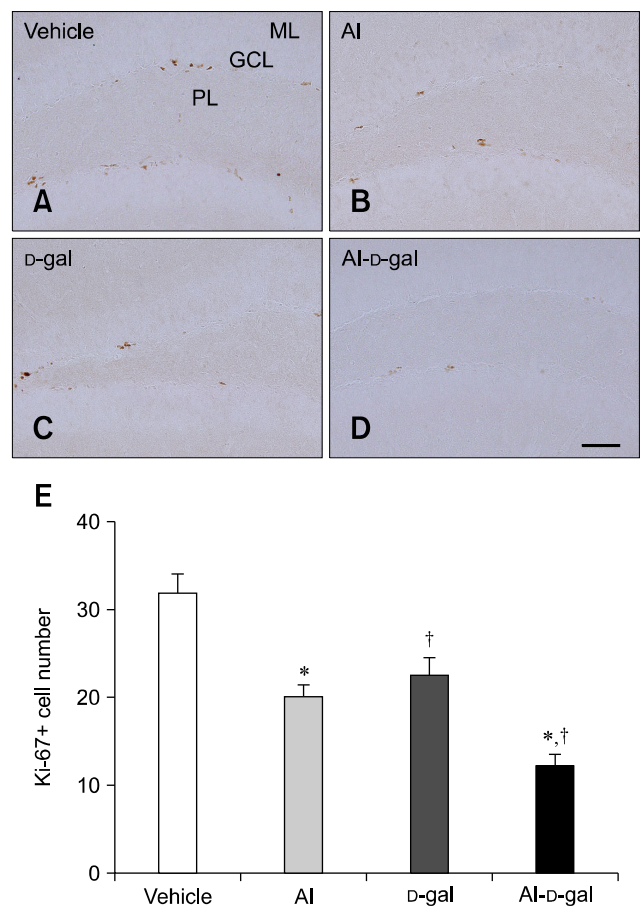
Fig. 3. Immunohistochemistry for Ki67 in the dentate gyrus of the vehicle (A), Al (B), D-gal (C), and Al-D-gal (D) groups. Ki67-immunoreactive nuclei are observed in the subgranular zone (arrows) of the dentate gyrus. Note that Ki67-immunoreactive nuclei decrease slightly in the Al and D-gal groups compared to the vehicle group. Ki67-immunoreactive nuclei are significantly reduced in the Al-D-gal group compared to the vehicle group. (E) Mean number of Ki67-positive nuclei per section in all groups ($n = 8$ per group; *$p < 0.05$ indicates a significant difference between vehicle/vehicle-D-gal and Al/Al-D-gal, †$p < 0.05$ indicates a significant difference between vehicle/vehicle-Al and D-gal/Al-D-gal). Data are presented as the mean ± SEM. Scale bar = 50 µm.

and mainly observed in the subgranular zone of the dentate gyrus (panels A–D in Fig. 3). In the vehicle group, the average number of Ki67-immunoreactive nuclei was highest, at 31.80 per section among groups (panel E in Fig. 3). Ki67-immunoreactive nuclei decreased dramatically in the Al and D-gal groups relative to the vehicle group (panels B and C in Fig. 3), with the average number of Ki67-immunoreactive nuclei being 20.00 (62.86% of the vehicle group, $p < 0.001$) and 22.60 (71.07% of the vehicle group, $p < 0.01$) per section, respectively (panel E in Fig. 3). In the Al-D-gal group, fewer Ki67-immunoreactive nuclei were detected in the dentate gyrus (panel D in Fig. 3), and the average number of Ki67-immunoreactive nuclei was lowest, 12.0 per section (panel E in Fig. 3). The level of Ki67-immunoreactive nuclei in the Al-D-gal group was 60.00% of those in the Al group ($p < 0.05$) and 53.10% of those in the D-gal group ($p < 0.01$) (panel E in Fig. 3).

Effects of Al and/or D-gal on neuroblast differentiation

DCX-immunoreactive neuroblasts were detected in the subgranular zone of the dentate gyrus. The complexity of the dendrites and dendritic branching pattern differed significantly among groups (Fig. 4). In the vehicle group, DCX-immunoreactive neuroblasts with well-branched dendrites were observed and dendrites extended into the molecular layer of the dentate gyrus (panels A and B in Fig. 4). In the Al and D-gal groups, fewer DCX-immunoreactive neuroblasts were observed and the complexity of dendrites was lower in these groups than the vehicle group (panels C–F in Fig. 4). DCX-immunoreactivity in the Al and D-gal groups was reduced to 70.37% ($p < 0.001$) and 78.40% ($p < 0.01$) of the vehicle group, respectively (panel I in Fig. 4). Additionally, the relative number of DCX-immunoreactive neuroblasts in the Al and D-gal groups was 79.27% ($p < 0.05$) and 85.51% ($p > 0.05$) of those in the vehicle group, respectively (panel J in Fig. 4). The lowest number of DCX-immunoreactive neuroblasts was detected in the Al-D-gal group (59.55% of the vehicle group), and this group also had the most poorly-developed dendrites (panels G, H, and J Fig. 4). Compared to the Al and D-gal groups, DCX immunoreactivity in this group was reduced significantly to 80.16% of the Al group ($p < 0.05$) and 71.95% of the D-gal groups ($p < 0.01$) (panel I in Fig. 4). Additionally, DCX immunoreactivity in this group was 56.41% of the vehicle group (panel I in Fig. 4). The relative number of DCX-immunoreactive neuroblasts in the Al-D-gal group was 75.13% of the Al group ($p < 0.05$) and 69.65% of the D-gal group ($p < 0.01$) (panel J in Fig. 4).

Effects of Al and/or D-gal on mature neurons

In all groups, NeuN-immunoreactive mature neurons were detected throughout the dentate gyrus, especially in the granule cell layer (Fig. 5). NeuN-immunoreactive mature neurons were
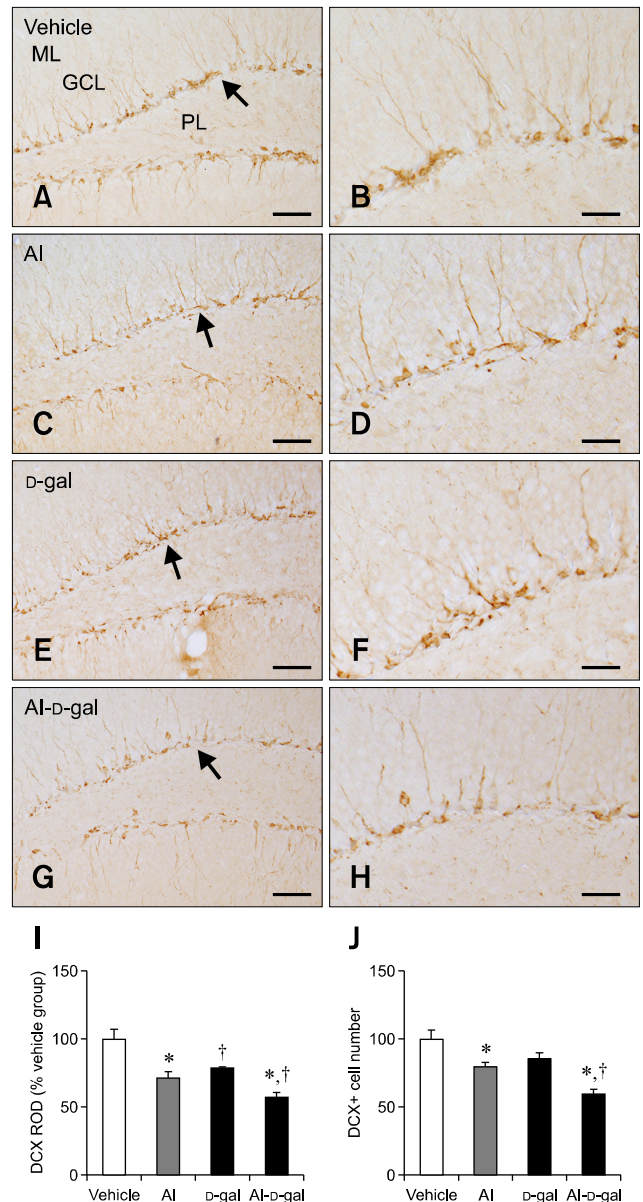

Fig. 4. Immunohistochemistry for doublecortin (DCX) in the dentate gyrus of the vehicle (A and B), Al (C and D), D-gal (E and F), and Al-D-gal (G and H) groups. DCX-immunoreactive neuroblasts are detected in the subgranular zone (arrows) of the dentate gyrus. Note the decreased DCX-immunoreactive neuroblasts in both the Al and D-gal groups compared to the vehicle group. DCX-immunoreactive neuroblasts are also significantly decreased in the Al-D-gal group compared to the vehicle group. (I) ROD demonstrated as a percentage of the vehicle group in DCX immunoreactivity per section in all groups. (J) Relative mean number of DCX-immunoreactive neuroblasts per section demonstrated as percentage of vehicle group ($n = 8$ per group; *$p < 0.05$ indicates a significant difference between vehicle/vehicle-D-gal and Al/ Al-D-gal, †$p < 0.05$ indicates a significant difference between vehicle/vehicle-Al and D-gal/Al-D-gal). Data are presented as the mean ± SEM. Scale bars = 50 μm (A, C, E and G), 25 μm (B, D, F and H).

similar in morphology and number in the Al and D-gal groups compared to the vehicle group ($p > 0.05$) (panels A–C, and E in Fig. 5). In the Al-D-gal group, NeuN-immunoreactive mature neurons were well preserved in morphology and the number in the dentate gyrus and its level did not differ from those in the Al and D-gal groups ($p > 0.05$) (panels D and E in Fig. 5).

Effects of Al and/or D-gal on lipid peroxidation

In all groups, 4-HNE immunoreactivity was mainly detected in the granular cell layer of the dentate gyrus. 4-HNE immunoreactivity was observed in the periphery of the cytoplasm (panels A–D in Fig. 6). 4-HNE immunoreactivity was increased significantly in the Al or D-gal groups compared to the control group (panels B and C in Fig. 6). 4-HNE immunoreactivity in the Al and D-gal groups was increased to

867.03% ($p < 0.001$) and 648.95% ($p < 0.01$) of that of the vehicle group, respectively (panel E in Fig. 6). 4-HNE immunoreactivity was higher in the Al group than that in the D-gal group. Dense 4-HNE immunoreactivity was observed in the cell membrane of the Al-D-gal group, and the 4-HNE immunoreactivity was highest among groups, being 968.71% of the vehicle group (panels D and E in Fig. 6). Compared to the Al and D-gal groups, 4-HNE immunoreactivity in this group was increased to 111.73% of that of the Al group and 149.27% of the D-gal group; however, this difference was not significant ($p > 0.05$) (panel E in Fig. 6).
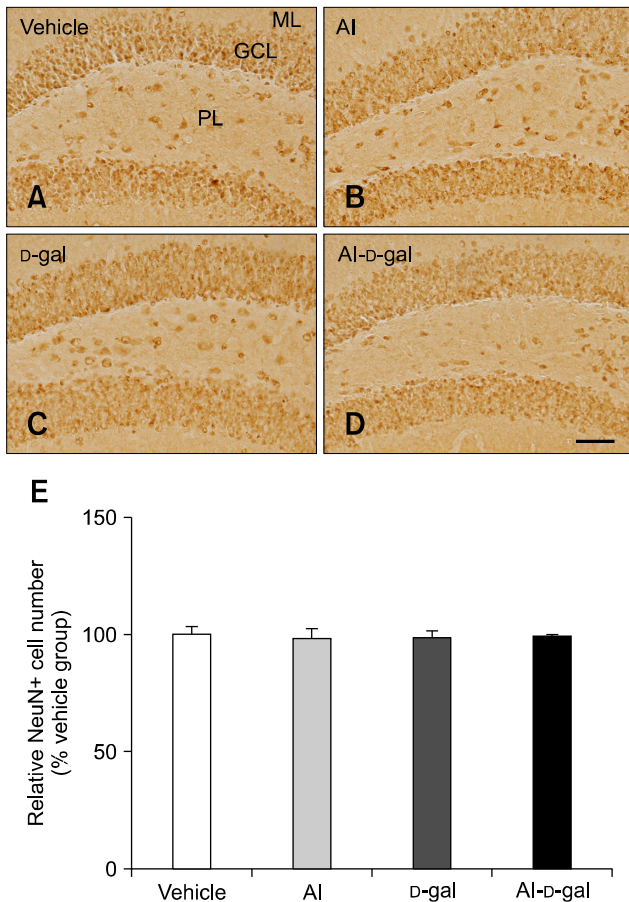

Fig. 5. Immunohistochemistry for NeuN in the dentate gyrus of the vehicle (A), Al (B), D-gal (C), and Al-D-gal (D) groups. NeuN-immunoreactive cells are mainly located in GCL of the dentate gyrus. NeuN-immunoreactive cell numbers are similar in all groups. (E) Relative number of NeuN-immunoreactive mature neurons demonstrated as percentage of vehicle group per section in all groups ($n = 8$ per group). Data are presented as the mean ± SEM. Scale bar = 50 μm.
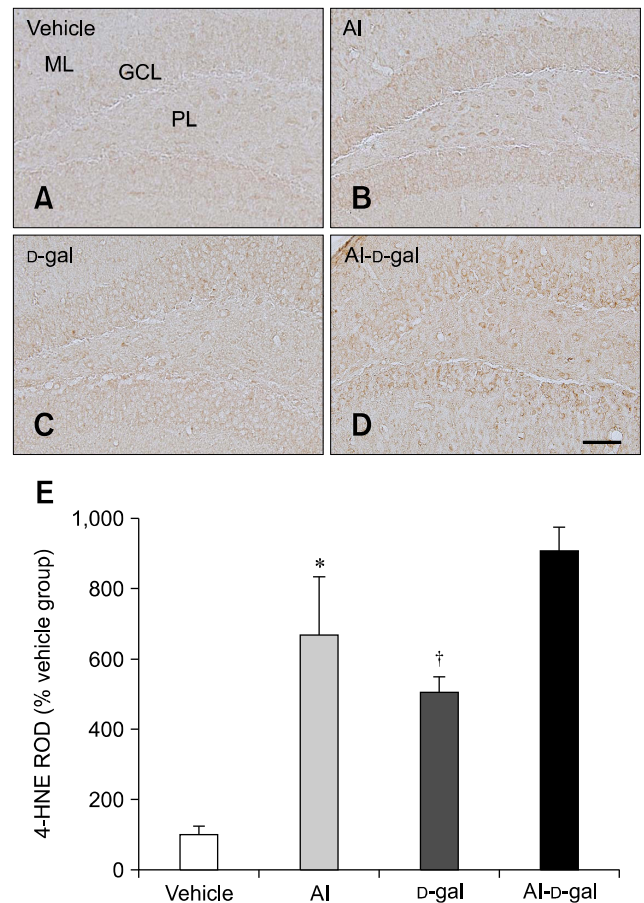

Fig. 6. Immunohistochemistry for 4-hydroxynonenal (4-HNE) in the dentate gyrus of the vehicle (A), Al (B), D-gal (C), and Al-D-gal (D) groups. 4-HNE immunoreactivity is mainly observed in GCL of the dentate gyrus. 4-HNE immunoreactivity is abundantly detected in the Al-D-gal group. (E) ROD demonstrated as percentage of vehicle group in 4-HNE immunoreactivity per section in all groups ($n = 8$ per group; *$p < 0.05$ indicates a significant difference between vehicle/vehicle-D-gal and Al/Al-D-gal, †$p < 0.05$ indicates a significant difference between vehicle/vehicle-Al and D-gal/Al-D-gal). Data are presented as the mean ± SEM. Scale bar = 50 μm.

Effects of Al and/or D-gal on SOD1 and SOD2

In all groups, SOD1 and SOD2 immunoreactivity were primarily detected in the granular cell layer of the dentate gyrus, although some immunoreactivity was also observed in the polymorphic layer of the dentate gyrus (panels A–D in Figs. 7 and 8). In the vehicle group, SOD1 and SOD2 immunoreactivity were the lowest among groups and Al or D-gal treatment increased the SOD1 (Al; 363.33% of the vehicle group, $p <$ 0.01, D-gal; 163.81% of the vehicle group, $p > 0.05$) and SOD2 (Al; 197.66% of the vehicle group, $p < 0.01$, D-gal; 158.59% of the vehicle group, $p < 0.05$) immunoreactivity in the dentate gyrus compared to that in the vehicle group, respectively (panel E in Figs. 7 and 8). In the Al-D-gal group, SOD1 immunoreactivity

was significantly increased to 176.45% of the Al ($p < 0.01$) and 391.36% of the D-gal ($p < 0.01$) groups (panel E in Fig. 7). Additionally, SOD2 immunoreactivity in this group was further increased to 125.01% of the Al ($p > 0.05$) and 155.80% of the D-gal ($p < 0.01$) groups (panel E in Figs. 7 and 8).

Discussion

Long-term exposure to Al is considered to be a factor contributing to neurodegeneration [13,33]. In addition, long-term treatment with D-gal potentially induces the phenotypes associated with aging by significantly reducing cell proliferation and neuroblast differentiation in the hippocampal dentate gyrus
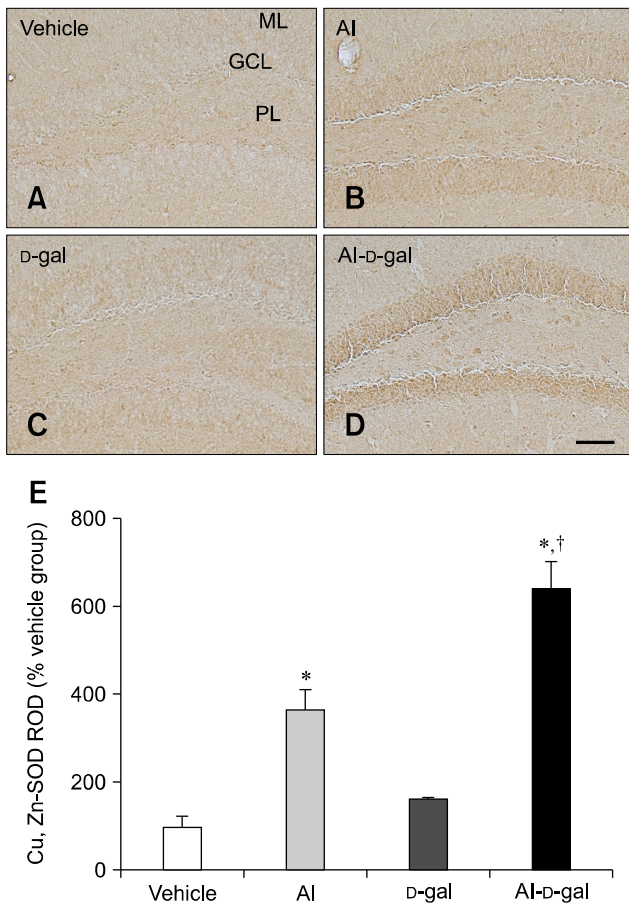

Fig. 7. Immunohistochemistry for superoxide dismutases (SOD)1 in the dentate gyrus of the vehicle (A), Al (B), D-gal (C), and Al-D-gal (D) groups. SOD1 immunoreactivity is mainly observed in GCL of the dentate gyrus. SOD1 immunoreactivity is increased in the GCL of the Al-D-gal group. (E) ROD demonstrated as a percentage of vehicle group in SOD1 immunoreactivity per section in all groups (n = 8 per group; *$p < 0.05$ indicates a significant difference between vehicle/vehicle-D-gal and Al/Al-D-gal, †$p < 0.05$ indicates a significant difference between vehicle/vehicle-Al and D-gal/Al-D-gal). Data are presented as the mean ± SEM. Scale bar = 50 μm.
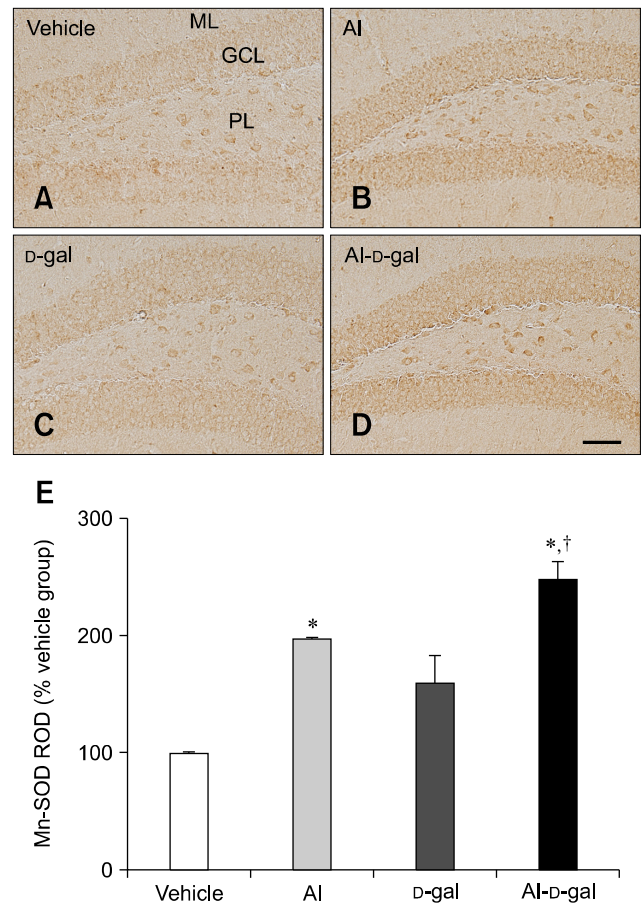

Fig. 8. Immunohistochemistry for SOD2 in the dentate gyrus of the vehicle (A), Al (B), D-gal (C), and Al-D-gal (D) groups. SOD2 immunoreactivity is mainly observed in GCL of the dentate gyrus. SOD2 immunoreactivity is increased in the GCL of the Al-D-gal group. (E) ROD demonstrated as a percentage of vehicle group in SOD2 immunoreactivity per section in all groups (n = 8 per group; *$p < 0.05$ indicates a significant difference between vehicle/vehicle-D-gal and Al/Al-D-gal, †$p < 0.05$ indicates a significant difference between vehicle/vehicle-Al and D-gal/Al-D-gal). Data are presented as the mean ± SEM. Scale bar = 50 μm.

[6,26]. However, it is not known whether Al treatment in D-gal injected mice aggravates impairment of adult neurogenesis. In the current study, we investigated the effects of subchronic (4 weeks) exposure to Al on adult neurogenesis in D-gal-treated mice.

First, we investigated physiological parameters such as body weight, food intake, and blood glucose levels in all groups. Body weight tended to increase in the vehicle-treated groups with increasing age, but to decrease in the Al treated groups with subsequent recovery at the end of the experiment. However, no significant difference in body weight was observed in response to Al and/or D-gal treatment. Additionally, food intake (calories consumed) was lower in the Al-treated groups than the non-Al-treated groups, especially at 7- and 8-weeks of age. Blood glucose levels did not differ among groups. These results suggest that intraperitoneal administration of Al negatively affected appetite and body mass gain, but that the effects of D-gal on these parameters were not prominent. However, Al treatment in D-gal-treated mice aggravated body mass loss without affecting other parameters. The intact blood glucose level means that the brain's essential energy source was not affected by either Al or D-gal treatment. However, intraperitoneal Al injection caused reduction of the blood glucose level in HFD-fed mice and a decrease in food intake and body weight [28].

We next immunostained for nestin, Ki67 and DCX to determine if subchronic Al and/or D-gal treatment affected neural stem cells, proliferating cells, and differentiating neuroblasts in the dentate gyrus. In this study, we detected a decrease in nestin, Ki67, and DCX immunoreactivity in both the Al and D-gal groups, compared to the vehicle group. These results suggest that Al and/or D-gal are acting as inhibitory factors on neural stem cells, cell proliferation, and neuroblast differentiation. However, the degree of reduction in these parameters was smaller in the D-gal group than the Al group. In addition, the reduction in immunoreactivity of these parameters was more prominent in the Al-D-gal group than in the Al and D-gal groups. The results presented here suggest that 4-week exposure to Al aggravates the negative effects of D-gal on adult hippocampal neurogenesis in an additive or synergistic way.

In previous studies, long-term treatment of D-gal resulted in hippocampal-dependent memory impairment and reduced adult hippocampal neurogenesis [6,26]. We confirmed that the degree of reduction induced by 4 weeks of treatment with D-gal was not as detrimental as longer-term D-gal treatments. However, additional Al exposure resulted in a more prominent decrease in neurogenesis in the dentate gyrus of D-gal mice. A 2-week exposure to Al in acidified water also impaired learning performance and reduced neural plasticity in salmon [15]. As one of the mechanisms of Al neurotoxicity, reactive oxygen species generation and the subsequent increase of lipid peroxidation causes damage to neuronal cells [40]. An overdose

of D-gal, like Al, increases the oxidative stress in neuronal cells through the formation of advanced glycation end products [18,34]. Al treatment via drinking water or intraperitoneal injection negatively affected adult hippocampal neurogenesis [27,28]. In addition to oxidative stress, further studies are required to clearly demonstrate whether Al-induced reduction in food intake influences neurogenesis in adult brain. Interestingly, Al in drinking water demonstrated its toxicity on adult hippocampal neurogenesis independent of physiological parameters [27].

To investigate whether 4 week exposure to Al and/or D-gal generates oxidative stress, we immunostained the lipid peroxidation product, 4-HNE, and confirmed the increase in the products of oxidative stress. Subsequently, hippocampal expression of antioxidant enzymes, SOD1 and SOD2, were increased in the Al or/and D-gal treated groups. An increased 4-HNE represents the treatment enhanced oxidative stress, and the increased cytosolic and mitochondrial SODs indicates that the hippocampal dentate gyrus is undergoing oxidative stress. Accordingly, previous studies reported that epilepsy or diabetes induced an oxidative stress accompanying increase of antioxidants as a long-term compensatory mechanism [11,16]. Unlike our present 4-week treatment of D-gal, 8-week exposure to D-gal caused a reduction in the SOD level [24], suggesting that the balance between ROS and antioxidant enzyme collapsed. At first, SOD increased to compensate; however, the continuous accumulation of oxidative stress exceeded the antioxidant system of the cell. Similarly, together with increased oxidative stress, a declining pattern of the antioxidant enzymes was confirmed in the brain with increasing age and development from the early to late stages of AD [2,36]. Additionally, Xiao et al. reported that 10 week combined treatment of Al (intragastric intubation, 20 mg/kg) and D-gal (subcutaneous injection, 120 mg/kg) resulted in AD pathology in the cortex and hippocampus [39]. In the present study, we used a different approached and injected Al at higher doses (40 mg/kg). Treatment using this method for longer than 4 weeks was lethal to C57BL/6J mice, with 90% mortality being observed at the end of the 8 week period. Therefore, to investigate long-term effects of Al on brain, we suggest that the administration route should be different or the dose reduced, and further differences in the susceptibility to Al toxicity among mouse strains should be considered.

Taken together, the results presented here indicate that neural stem cells, as well as their proliferation and neuronal differentiation during adult neurogenesis are negatively affected by Al or/and D-gal via oxidative stress, although mature neurons do not show any significant losses in response to Al or/and D-gal. Therefore, Al may be an environmental hazard that affects adult hippocampal neurogenesis in animals, and Al toxicity increased with oxidative stress related to the aging process.

Acknowledgments

Conflict of Interest

There is no conflict of interest.

References

1. **Abdel Moneim AE, Othman MS, Mohmoud SM, El-Deib KM.** Pomegranate peel attenuates aluminum-induced hepatorenal toxicity. Toxicol Mech Methods 2013, **23**, 624-633.

2. **Ansari MA, Scheff SW.** Oxidative stress in the progression of Alzheimer disease in the frontal cortex. J Neuropathol Exp Neurol 2010, **69**, 155-167.

3. **Ball MJ, Fisman M, Hachinski V, Blume W, Fox A, Kral VA, Kirshen AJ, Fox H, Merskey H.** A new definition of Alzheimer's disease: a hippocampal dementia. Lancet 1985, **1**, 14-16.

4. **Bignucolo A, Lemire J, Auger C, Castonguay Z, Appanna V, Appanna VD.** The molecular connection between aluminum toxicity, anemia, inflammation and obesity: therapeutic cues. In: Silverberg D (ed.). Anemia. pp. 403-424, InTech, Rijeka, 2012.

5. **Crapo JD, Oury T, Rabouille C, Slot JW, Chang LY.** Copper, zinc superoxide dismutase is primarily a cytosolic protein in human cells. Proc Natl Acad Sci U S A 1992, **89**, 10405-10409.

6. **Cui X, Zuo P, Zhang Q, Li X, Hu Y, Long J, Packer L, Liu J.** Chronic systemic D-galactose exposure induces memory loss, neurodegeneration, and oxidative damage in mice: protective effects of R-α-lipoic acid. J Neurosci Res 2006, **84**, 647-654.

7. **Eisenreich SJ.** Atmospheric input of trace metals to Lake Michigan. Water Air Soil Pollut 1980, **13**, 287-301.

8. **Fanselow MS, Dong HW.** Are the dorsal and ventral hippocampus functionally distinct structures? Neuron 2010, **65**, 7-19.

9. **Filipek LH, Nordstrom DK, Ficklin WH.** Interaction of acid mine drainage with waters and sediments of West Squaw Creek in the West Shasta Mining District, California. Environ Sci Technol 1987, **21**, 388-396.

10. **Franklin KBJ, Paxinos G.** The mouse brain in stereotaxic coordinates. Academic Press, San Diego, 1997.

11. **Freitas RM.** Investigation of oxidative stress involvement in hippocampus in epilepsy model induced by pilocarpine. Neurosci Lett 2009, **462**, 225-229.

12. **Ganrot PO.** Metabolism and possible health effects of aluminum. Environ Health Perspect 1986, **65**, 363-441.

13. **Gauthier E, Fortier I, Courchesne F, Pepin P, Mortimer J, Gauvreau D.** Aluminum forms in drinking water and risk of Alzheimer's disease. Environ Res 2000, **84**, 234-246.

14. **Gómez M, Esparza JL, Cabré M, García T, Domingo JL.** Aluminum exposure through the diet: metal levels in AβPP transgenic mice, a model for Alzheimer's disease. Toxicology 2008, **249**, 214-219.

15. **Grassie C, Braithwaite VA, Nilsson J, Nilsen TO, Teien HC, Handeland SO, Stefansson SO, Tronci V, Gorissen M, Flik G, Ebbesson LO.** Aluminum exposure impacts brain plasticity and behavior in Atlantic salmon (*Salmo salar*). J Exp Biol 2013, **216**, 3148-3155.

16. **Grillo CA, Piroli GG, Rosell DR, Hoskin EK, Mcewen BS, Reagan LP.** Region specific increases in oxidative stress and superoxide dismutase in the hippocampus of diabetic rats subjected to stress. Neuroscience 2003, **121**, 133-140.

17. **Harris WR, Berthon G, Day JP, Exley C, Flaten TP, Forbes WF, Kiss T, Orvig C, Zatta PF.** Speciation of aluminum in biological systems. J Toxicol Environ Health 1996, **48**, 543-568.

18. **Hsieh HM, Wu WM, Hu ML.** Soy isoflavones attenuate oxidative stress and improve parameters related to aging and Alzheimer's disease in C57BL/6J mice treated with D-galactose. Food Chem Toxicol 2009, **47**, 625-632.

19. **Hyman BT, Van Hoesen GW, Damasio AR, Barnes CL.** Alzheimer's disease: cell-specific pathology isolates the hippocampal formation. Science 1984, **225**, 1168-1170.

20. **Krewski D, Yokel RA, Nieboer E, Borchelt D, Cohen J, Harry J, Kacew S, Lindsay J, Mahfouz AM, Rondeau V.** Human health risk assessment for aluminium, aluminium oxide, and aluminium hydroxide. J Toxicol Environ Health B Crit Rev 2007, **10** (Suppl), 1-269.

21. **Kruman I, Bruce-Keller AJ, Bredesen D, Waeg G, Mattson MP.** Evidence that 4-hydroxynonenal mediates oxidative stress-induced neuronal apoptosis. J Neurosci 1997, **17**, 5089-5100.

22. **Lei M, Hua X, Xiao M, Ding J, Han Q, Hu G.** Impairments of astrocytes are involved in the D-galactose-induced brain aging. Biochem Biophys Res Commun 2008, **369**, 1082-1087.

23. **Lisman J.** Formation of the non-functional and functional pools of granule cells in the dentate gyrus: role of neurogensis, LTP and LTD. J Physiol 2011, **589**, 1905-1909.

24. **Lu J, Zheng YL, Wu DM, Luo L, Sun DX, Shan Q.** Ursolic acid ameliorates cognition deficits and attenuates oxidative damage in the brain of senescent mice induced by D-galactose. Biochem Pharmacol 2007, **74**, 1078-1090.

25. **Mićić DV, Petronijević ND, Vucetić SS.** Superoxide dismutase activity in the mongolian gerbil brain after acute poisoning with aluminum. J Alzheimers Dis 2003, **5**, 49-56.

26. **Nam SM, Choi JH, Yoo DY, Kim W, Jung HY, Kim JW, Kang SY, Park J, Kim DW, Kim WJ, Yoon YS, Hwang IK.** *Valeriana officinalis* extract and its main component, valerenic acid, ameliorate D-galactose-induced reductions in memory, cell proliferation, and neuroblast differentiation by reducing corticosterone levels and lipid peroxidation. Exp Gerontol 2013, **48**, 1369-1377.

27. **Nam SM, Kim JW, Yoo DY, Jung HY, Choi JH, Hwang IK, Seong JK, Yoon YS.** Reduction of adult hippocampal neurogenesis is amplified by aluminum exposure in a model of type 2 diabetes. J Vet Sci 2016, **17**, 13-20.

28. **Nam SM, Kim JW, Yoo DY, Kim W, Jung HY, Hwang IK, Seong JK, Yoon YS.** Additive or synergistic effects of aluminum on the reduction of neural stem cells, cell proliferation, and neuroblast differentiation in the dentate gyrus of high-fat diet-fed mice. Biol Trace Elem Res 2014, **157**, 51-59.

29. **Nayak P.** Aluminum: impacts and disease. Environ Res 2002, **89**, 101-115.

30. **Poirier J, Semple H, Davies J, Lapointe R, Dziwenka M, Hiltz M, Mujibi D.** Double-blind, vehicle-controlled randomized twelve-month neurodevelopmental toxicity study of common aluminum salts in the rat. Neuroscience 2011, **193**, 338-362.

31. **Priest ND.** The biological behaviour and bioavailability of aluminium in man, with special reference to studies employing aluminium-26 as a tracer: review and study update. J Environ Monit 2004, **6**, 375-403.

32. **Salmon AB, Richardson A, Pérez VI.** Update on the oxidative stress theory of aging: does oxidative stress play a role in aging or healthy aging? Free Radic Biol Med 2010, **48**, 642-655.

33. **Savory J, Herman MM, Ghribi O.** Mechanisms of aluminum-induced neurodegeneration in animals: implications for Alzheimer's disease. J Alzheimers Dis 2006, **10**, 135-144.

34. **Song X, Bao M, Li D, Li YM.** Advanced glycation in D-galactose induced mouse aging model. Mech Ageing Dev 1999, **108**, 239-251.

35. **Southorn PA, Powis G.** Free radicals in medicine. I. Chemical nature and biologic reactions. Mayo Clin Proc 1988, **63**, 381-389.

36. **Venkateshappa C, Harish G, Mahadevan A, Srinivas Bharath MM, Shankar SK.** Elevated oxidative stress and decreased antioxidant function in the human hippocampus and frontal cortex with increasing age: implications for neurodegeneration in Alzheimer's disease. Neurochem Res 2012, **37**, 1601-1614.

37. **Walton JR.** Brain lesions comprised of aluminum-rich cells that lack microtubules may be associated with the cognitive deficit of Alzheimer's disease. Neurotoxicology 2009, **30**, 1059-1069.

38. **Weisiger RA, Fridovich I.** Mitochondrial superoxide dismutase. Site of synthesis and intramitochondrial localization. J Biol Chem 1973, **248**, 4793-4796.

39. **Xiao F, Li XG, Zhang XY, Hou JD, Lin LF, Gao Q, Luo HM.** Combined administration of *D*-galactose and aluminium induces Alzheimer-like lesions in brain. Neurosci Bull 2011, **27**, 143-155.

40. **Xie CX, Mattson MP, Lovell MA, Yokel RA.** Intraneuronal aluminum potentiates iron-induced oxidative stress in cultured rat hippocampal neurons. Brain Res 1996, **743**, 271-277.